

# Cell Surface Engineering with Edible Protein Nanoshells

Irina Drachuk, Olga Shchepelina, Svetlana Harbaugh, Nancy Kelley-Loughnane, Morley Stone, and Vladimir V. Tsukruk\*

**N**atural protein (silk fibroin) nanoshells are assembled on the surface of *Saccharomyces cerevisiae* yeast cells without compromising their viability. The nanoshells facilitate initial protection of the cells and allow them to function in encapsulated state for some time period, afterwards being completely biodegraded and consumed by the cells. In contrast to a traditional methanol treatment, the gentle ionic treatment suggested here stabilizes the shell silk fibroin structure but does not compromise the viability of the cells, as indicated by the fast response of the encapsulated cells, with an immediate activation by the inducer molecules. Extremely high viability rates (up to 97%) and preserved activity of encapsulated cells are facilitated by cytocompatibility of the natural proteins and the formation of highly porous shells in contrast to traditional polyelectrolyte-based materials. Moreover, in a high contrast to traditional synthetic shells, the silk proteins are biodegradable and can be consumed by cells at a later stage of growth, thus releasing the cells from their temporary protective capsules. These on-demand encapsulated cells can be considered a valuable platform for biocompatible and biodegradable cell encapsulation, controlled cell protection in a synthetic environment, transfer to a device environment, and cell implantation followed by biodegradation and consumption of protective protein shells.

## 1. Introduction

Biopolymers are widely utilized for the formation of coatings, scaffolds or matrices for the integration of cells into synthetic environments or for implantation in tissue scaffolds.<sup>[1–5]</sup> Functionalization of the coatings by various biomacromolecules results in hybrid components, which have potential for controlled biochemical delivery and attachment to specific targets.<sup>[6,7]</sup> The inherent biocompatibility of biopolymer

coatings with the potential to preserve viability and activity of cells after encapsulation demonstrates a striking contrast compared to synthetic polymer shells with common known issues such as cytotoxicity, non-biodegradability, and low permeability.<sup>[8–10]</sup>

Recently, developments in micro- and bioelectronics such as cell-based biosensors, thermal and chemical sensors, biomimicking devices, and biochip technologies have emerged.<sup>[11–14]</sup> Demands for long-term cell viability, functionality, and sustainability in artificial environment (hostile nature) such as inorganic electrodes or synthetic cytotoxic matrices are important for many of these developments. Robust living cell-based biosensors with long-term shelf life can show high real-time sensitivity detection in response to a target analyte,<sup>[15]</sup> protection from ex vivo environment,<sup>[16]</sup> and preserved viability/activity.<sup>[8]</sup> Motivation factors behind encapsulation of living cells in protein shells also include the ability to reengineer the surface of the cell with proteins allowing for control of interactions with ex vivo environment, such as immobilization on patterned synthetic surfaces,<sup>[17]</sup>

I. Drachuk, Dr. O. Shchepelina, Prof. V. V. Tsukruk

School of Materials Science and Engineering

Georgia Institute of Technology

Atlanta, GA 30332, USA

E-mail: vladimir@mse.gatech.edu

Dr. S. Harbaugh, Dr. N. Kelley-Loughnane, Dr. M. Stone

Air Force Research Laboratory

Directorate of Human Effectiveness

Wright-Patterson AFB, Dayton, OH 45433, USA

DOI: 10.1002/smll.201202992



controlled adhesion of coated cells on surfaces with different affinities,<sup>[18]</sup> or guided/directed location and growth of cells.<sup>[19]</sup>

One of the extensively studied natural polymers, silk fibroin, has been successfully used for cell encapsulation. Silk-based materials have been exploited for tissue engineering scaffolds and matrices due to their biodegradation, biocompatibility, excellent mechanical properties, and versatility in further functionalization.<sup>[20,21]</sup> Due to long-term stability and low inflammatory or immune response *in vivo*, a number of mammalian cells and tissues were encapsulated in silk scaffolds. For example, by systematically changing silk material concentration during extraction and processing, cartilage cells were encapsulated in silk hydrogels with the full maintenance of cell viability.<sup>[20,22]</sup> Another example of successful *in situ* gelation and cell entrapment was reported by synthesizing ionomer-functionalized silk biopolymers and mixing them in equal amounts in the presence of fibroblast cells at physiologically relevant conditions in order to produce instant hydrogels with entrapped cells. By taking advantage of genetically engineered silk-elastin polymers that undergo sol-to-gel transitions within minutes, injectable matrices can be used for delivery of cell-based therapeutics.<sup>[23]</sup> Such hydrogels were proven to be viable scaffolds for the *in vivo* chondrogenesis if stimulated by growth factors but were unfavorable for the diffusion of the produced extracellular matrix proteins due to limited flexibility of the hydrogel scaffold and free volume into which extracellular proteins could be deposited. Large volumes and limited porosity of bio-enabled hydrogels are the major obstacles for cell-based therapeutics or bio-sensing applications when rapid responsiveness of the encapsulated cells should be attained.

The formation of ultrathin silk coatings on cell surfaces has never been explored despite the fact that robust silk films have been widely demonstrated.<sup>[24]</sup> In this context, layer-by-layer (LbL) self-assembly has been explored not only between oppositely-charged polyelectrolytes, but also

in hydrogen-bonded or hydrophobic systems.<sup>[1,25–28]</sup> These nanoshells efficiently reduce material volume while retaining the presence of the protective coating,<sup>[8,29]</sup> create semipermeable artificial membranes for the efficient exchange of nutrients and signaling molecules and efficiently release waste products. Moreover, these coatings might inhibit molecular recognition<sup>[30,31]</sup> or guide the delivery of the cargo.<sup>[32–36]</sup>

The transition of a random silk fibroin that is soluble in water (silk I) to a highly stable and organized structure that is insoluble in water (silk II), which is required to form stable silk matrices, can be accomplished by several processing methods including dehydration by using organic solvents, surfactants, initiators or crosslinking agents, or physical factors (shear, sonication, temperature).<sup>[37–41]</sup> It also has been shown that the extent of protein aggregation can be controlled by the concentration of kosmotropic salts or ions.<sup>[37]</sup> However, despite prior investigations on bulk hydrogelation of native silk fibroin by salting-out processes<sup>[37–39]</sup> and examples of stable microgels and thin films,<sup>[40,41]</sup> no attempts directed at exploiting silk fibroin for surface cell engineering have been reported.

In this paper, we report on the formation of stable silk nanoshells around living cells by inducing secondary structure transitions directly on the cell surfaces to lock in non-soluble silk conformation by cell-friendly ionic treatment (**Figure 1**). During LbL assembly of silk nanoscale shells,  $\beta$ -sheet rich physical crosslinks are formed as a result of the salting-out process complemented by the shear-thinning effect as have been proved by extensive studies from Kaplan and Scheibel groups.<sup>[20,22,37–39,42,43]</sup> Greatly enhanced viability of yeast cells encapsulated in ~10 nm silk shells of up to 97% is in accord with preserved metabolic activity and fast response to inducer molecules. This high viability demonstrates the biocompatibility of the salting-out process and the formation of porous protein shells for efficient uptake of the nutrients. Moreover, in high contrast to traditional synthetic nanoshells widely used for cell encapsulation, the protein shells suggested here are biodegradable and consumed by cells after completing their protective role, thus facilitating efficient cell post-release critical for seamless implantation (Figure 1).

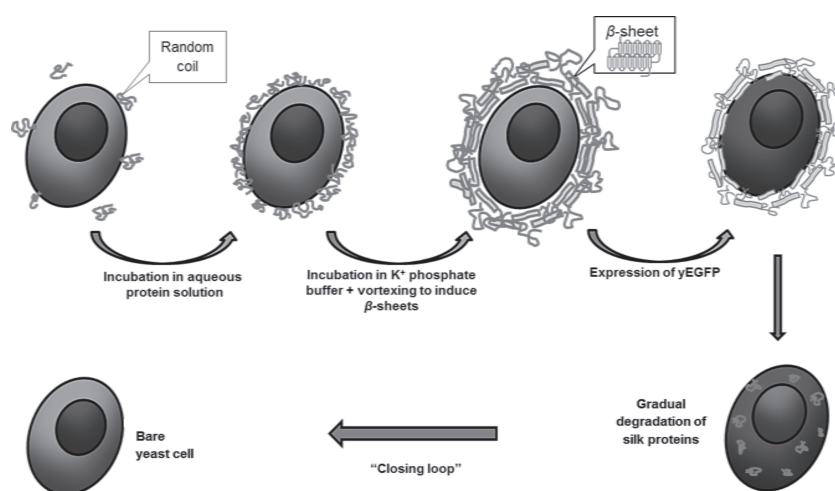
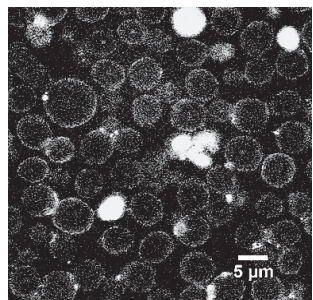


**Figure 1.** Schematic representation of silk-on-silk LbL deposition to form silk II rich structure on the surface of yeast cells, followed by expression of yEGFP after incubation in media supplemented with inducer molecule (galactose) after formation of silk nanoshells; gradual biodegradation and internalization of silk proteins and returning to the bare state without coatings.

## 2. Results and Discussion

In order to minimize cytotoxicity and avoid prolonged exposure of the cells to potentially toxic processing conditions, we explored the formation of stable silk shells produced by an all-aqueous salting-out process induced by a kosmotropic phosphate buffer. In order to assess the effect of salts on the viability of yeast cells and to optimize molar concentrations, we performed LbL encapsulation of *Saccharomyces cerevisiae* yeast cells in locked in silk shells induced by treatment with either sodium phosphates, potassium

(a)



(b)

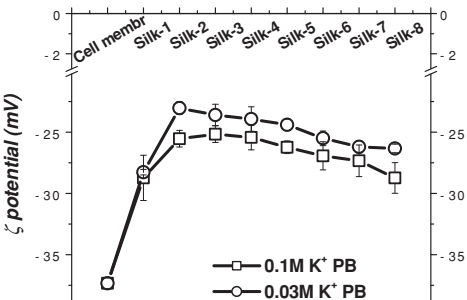


**Figure 2.** a) Confocal images of yeast cells encapsulated in silk-on-silk shells as visualized by fluorescently labeled silk (silk-*co*-Alexa532) deposited as the top layer; b)  $\zeta$ -potential of yeast cells after deposition of each silk layer (e.g., Silk-1, Silk-2) and treatment with  $K^+$  phosphate buffer ( $K^+$  PB) for 10 min.

phosphates, or phosphates supplemented with calcium chloride (Figure 1).<sup>[43]</sup>

The formation of stable silk shells is evident as strong fluorescent emission (red) was observed around the periphery of yeast cells (Figure 2a). It also confirms the integrity of the silk coatings and the formation of stable silk nanoshells via the salting-out process by a moderately strong  $K^+$  phosphate buffer and preservation of non-soluble silk nanoshells (Figure S1). Afterwards, successful assembly of silk LbL shells was monitored by measuring  $\zeta$ -potential after deposition and the salting-out procedure (Figure 2b). Control yeast cells possessed strong negative  $\zeta$ -potential of -38 mV. After assembly of silk proteins,  $\zeta$ -potential was reduced to the range of -22 to -28 mV regardless of the molarity of potassium phosphates (0.1 M or 0.03 M) or number of deposition cycles, suggesting the stabilization of protein shells by salts and accumulation of silk on the cell surfaces.

**Figure 3** demonstrates the viability of encapsulated cells in response to the treatment with different salts or the traditional methanol cure (control sample). With the control specimen, even a low methanol concentration and brief washing steps (5–10 sec), which are necessary to induce

$\beta$ -sheet conformations, result in a significant reduction of cell viability (below 40%) that confirmed incompatibility of the traditional methanol treatment with cell surface engineering (Figure 3). As a next step, negative controls were assessed to determine the viability of yeast cells incubated in the solutions of phosphate buffers with different ionic strengths (0.1 M or 0.03 M) (Figure 3, Figure S1). These results show that salts alone do not compromise cell activity, since bare cells demonstrated 100% viability and metabolic activity. On the other hand, after encapsulation and treatment with phosphate buffers the viability rate varied depending on the strength of molarity and the type

of buffer. Potassium phosphate at physiologically relevant conditions (0.03 M, pH 5.3 for yeast cells) promoted higher cell viability rates in comparison to sodium phosphate of the same molarity or potassium phosphate of a higher molarity (0.1 M, pH 5.3) (Figure 3).

Alternatively, a live-dead assay (Figure 3a) or a bioreduction assay of resazurin (Figure 3b) complemented each other, showing excellent viability rates: 97% (live-dead test) and about 92% (resazurin test) for cells encapsulated in 8 layers of silk nanoshells. In contrast, viability rates for cells encapsulated in silk shells with the same composition of layers but incubated in higher molarity of phosphates (0.1 M) were moderately reduced to 80% (live-dead test) or 67% (resazurin test) (Figure S1). The difference in viability rates can be explained by the nature of susceptibility testing. While general survivability of cells is represented by live-dead test, the level of metabolic activity of viable cells is assessed by bioreduction of resazurin, where the function/activity of even membrane-preserved cells could be significantly affected. Hence, assessment with two independent cytotoxicity assays allowed us to demonstrate not only high survivability rate (97%) of silk-modified cells using physiologically relevant salt treatment, but also showed consistent and significant retention of metabolic activity after the process of encapsulation (92%). With increased concentration of phosphate buffers during incubation (0.5 M, pH 5.3), significant aggregation of cells was observed, indicating limiting conditions of the salting-out process and the need for a moderate strength molarity of phosphate buffers.

In vivo studies suggested that  $Ca^{2+}$  (strong kosmotrope) plays an important role in stabilizing the silk fibroin protein in order to yield proper folding of the protein and to obtain the silk II conformation.<sup>[38,43]</sup> However, the effect of calcium ions even in low concentrations (0.05 M) supplemented with either  $K^+$  or  $Na^+$  phosphates had an adverse effect on cell viability and resulted in significant reduction

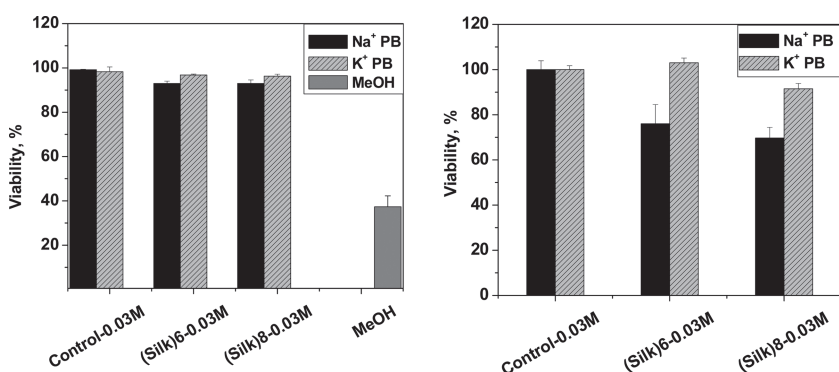
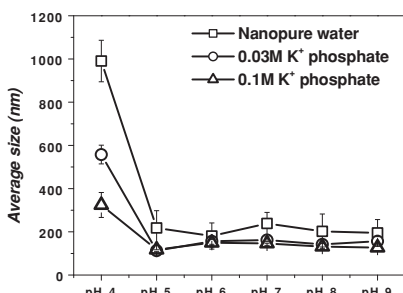


**Figure 3.** Viability rates of yeast cells encapsulated in silk shells assessed with a) live-dead and b) bioreduction of resazurin assays. Cells have been encapsulated in different number of layers (6 and 8) and treated by salting-out in sodium or potassium phosphate buffers of 0.03 M molarity after deposition of each layer of silk. Control cells have been incubated in 0.03 M solutions of  $Na^+$  or  $K^+$  phosphate buffers ( $Na^+$  PB or  $K^+$  PB) (Control-0.03M). For comparison, viability of yeast cells encapsulated in 8 layers of silk and treated with methanol after deposition of each layer is presented (MeOH).

(a)



(b)

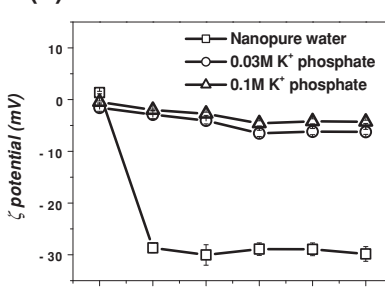


Figure 4. Change in average a) size and b)  $\zeta$ -potential of silk micelles as a function of pH in potassium phosphate buffers of different molarity and in Nanopure water.

of viability rates to 9.5% (Figure S1). Hence, the formation of stable silk nanoshells on cell surfaces was limited to the salting-out process induced by phosphate buffers (either  $\text{Na}^+$  or  $\text{K}^+$ ). Even though  $\text{Na}^+$  and  $\text{K}^+$  ions are placed next to each other in the Hofmeister series and are roughly neutral, with the former being a very weak kosmotrope and the latter a weak chaotrope, it can be assumed that  $\text{Na}^+$  along with phosphate (very strong kosmotrope) can efficiently stabilize proteins or membranes and strengthen hydrogen bonding and hydrophobic interactions during the salting-out process. However, viability rates were significantly lower compared to  $\text{K}^+$  phosphate after encapsulation in silk nanoshells and incubation in a  $\text{Na}^+$  phosphate buffer of comparable molarity (Figure 3). On the other hand, combination of potassium with the phosphate anion demonstrated the most cytocompatibility, where the metabolic activation in addition to the high viability of encapsulated cells has been preserved.

Such behavior can be caused by matching extracellular conditions of potassium ions (0.03 M, pH 5.3), which correlates well with intrinsic conditions essential for active transport across the cell membrane and hence for preservation of metabolic activity of the cells.<sup>[44]</sup> Alternatively, potassium is found to be significantly less efficient in binding affinity to protein surfaces containing  $\text{COO}^-$  groups than  $\text{Na}^+$ .<sup>[45]</sup> Protein hydrophilic domains can be impaired by  $\text{Na}^+$ , which can destabilize the proteins and lead to their unfolded structure and thus reduced cell viability.<sup>[45]</sup> Pairing a chaotropic cation ( $\text{K}^+$ ) with a kosmotropic anion ( $\text{HPO}_4^{2-}$ ) is responsible for the preferential hydration of the protein, which enables enhanced water-protein interactions.<sup>[46]</sup>

We have also assessed the effect of pH in combination with the salting-out efficiency of potassium phosphate buffer on sol-gel transitions of silk protein. **Figure 4** demonstrates the change in size and  $\zeta$ -potential of the protein micelles as a function of pH for very dilute silk (0.1% w/v) and salt concentration (0.03 M and 0.1 M). The pH was adjusted by mixing mono- and dibasic potassium phosphate solutions from pH 4 up to pH 9, which are almost identical in their salting-out efficiency.<sup>[47]</sup> Dynamic light scattering (DLS) measurements showed that dramatic changes in the protein dimensions occurred below isoelectric point (pI) for the N-terminus for both molar concentrations (0.1 M and 0.03 M) of buffers when compared to Nanopure water (Figure 4a). At acidic conditions (below pH 5), we observed the formation

of micelles of 1  $\mu\text{m}$ , 200 nm, and 300 nm in Nanopure water, and buffer solutions of 0.03 M and 0.1 M respectively. Above pH 5, significant five-fold reduction in the size of micellar structures was observed (Figure 4). Noticeably, salt-induced transitions resulted in efficient  $\beta$ -sheet formation.<sup>[37,48]</sup> In the range of pH 5–9, silk micelles were  $110 \pm 15$  nm in diameter in buffer solutions and  $180 \pm 20$  nm across in Nanopure water (Figure 4). Increasing the phosphate concentration from 0.03 M to 0.1 M resulted in decrease sizes by 15%, suggesting some additional compaction of silk micelles.

Alternatively,  $\zeta$ -potential measurements of silk micelles produced at different pH values showed the protonated states of carboxylic groups below pH 5 in pure water (Figure 4b). Above pH 5, the deprotonation process results in large negative surface potential. These results confirm the isoelectric point of 4.6 known from literature for one of the terminal silk domains.<sup>[38,47,49]</sup> Indeed, the N-terminus, a large hydrophilic domain and light chain, displays a predominance of negatively charged amino acid side chains and have pI value of 4.6 and 5.06, respectively.<sup>[49]</sup> On the other hand, the C-terminus has a predominance of positive charges and a pI value of 10.5. The presence of salt ions can significantly screen highly negative surface potential of silk fibroin and shift the apparent isoelectric point for the N-terminus to pH 6. Overall, one can conclude that even a moderate ionic strength phosphate buffers (0.03 M) induces the silk transformation in the neutral pH range with a significant spike in transitions at pH 4.

A similar trend has been observed for significantly higher concentrations of silk fibroin (between 0.25 mg mL<sup>-1</sup> and 8 mg mL<sup>-1</sup>), as well as higher concentrations of potassium phosphate (from 0.5 M to 1.25 M).<sup>[47,50]</sup> To independently confirm the stability of different silk layers, we fabricated silk films using the dip-assisted LbL method and exposed them to the solutions of  $\text{K}^+$  phosphate buffers of different strength (0.03 M, 0.1 M, or 0.5 M, pH 5.5), followed by brief washing in Nanopure water (Figure S2). The resulting high retention of silk materials showed that even lower molarities of  $\text{K}^+$  phosphate buffer promoted silk film stabilization lower but comparable than that of the traditional methanol treatment.

Isoelectric points for the silk fibroin can be related to the transitions in secondary structure of silk nanoshells. In pure water below pH 5, the degree of protonation of carboxyl groups for the N-terminus and for the light chain in silk fibroin significantly increases, promoting hydrogen bonding. In the presence of salts, the formation of micelles is induced by additional ionic interactions of charged protonated basic groups and phosphate ions under these pH conditions. With an increase in pH from pH 6 to 9 in the absence of salts, the degree of deprotonation for both carboxylic and basic groups increased with predominant role of carboxyl groups (negative values of surface potential). Alternatively, the presence of salt screens ionic interactions and promotes further transformation due to increased hydrophobic interactions.

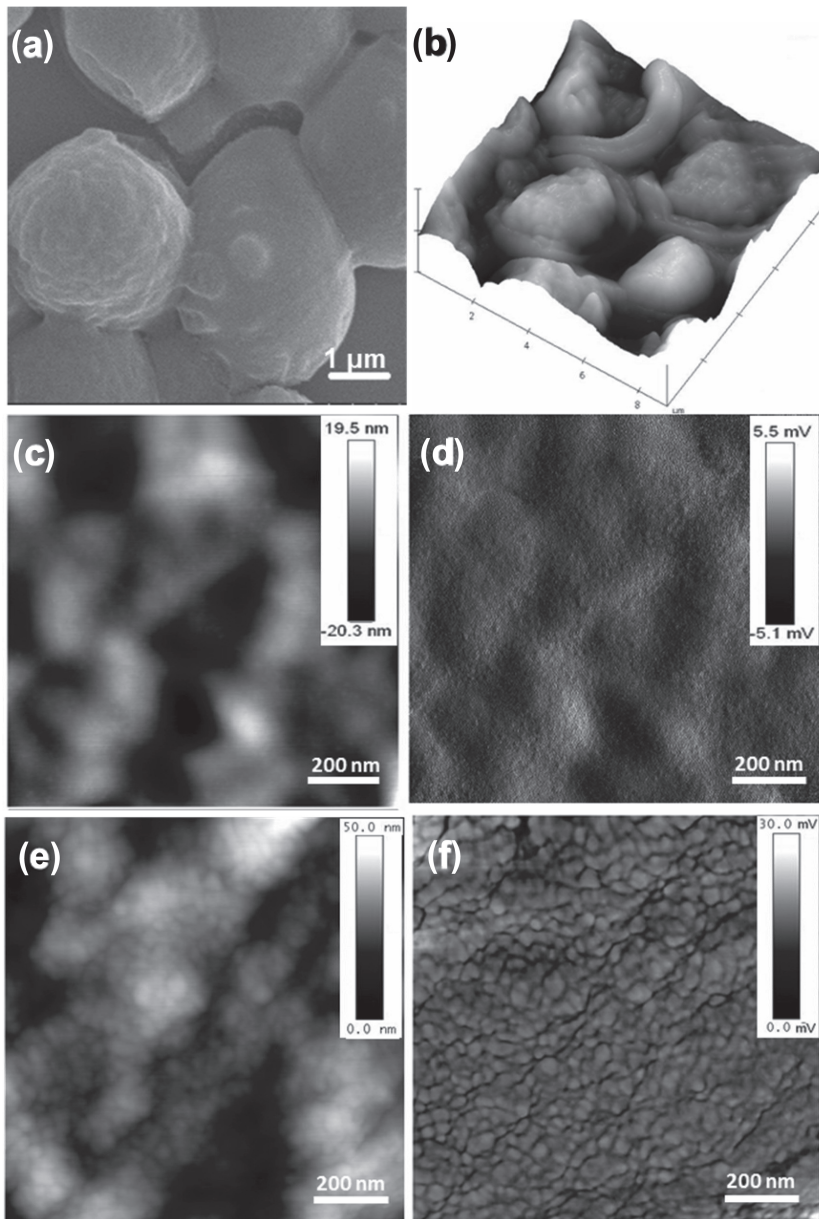


**Figure 5.** a) SEM images of yeast cells encapsulated in (silk)<sub>8</sub> shells and treated with 0.03 M K<sup>+</sup> phosphate buffer (pH 5.3); b) Reconstructed 3D AFM surface image of several cells encapsulated with (silk)<sub>8</sub> shells (Z-scale is 1  $\mu$ m); c–f) AFM images showing surface morphology of c,d) bare yeast cells and e,f) cells encapsulated in (silk)<sub>8</sub> shells. Figures c,e) are height (Z-scale is 50 nm) and d,f) are phase images.

Micelles formed under these conditions are smaller with faster gelation of silk protein near neutral pH. Based on these measurements, we optimized the conditions for gentle and cell-friendly stabilization of silk shells by salting-out in 0.03 M potassium phosphate buffer (pH 5.3).

Atomic force microscopy (AFM) and scanning electron microscopy (SEM) analysis confirms the formation of uniform silk coatings on cells (**Figure 5**). Increased aggregation of silk shells and a net-like appearance are characteristics of these shells a modest increase in microroughness from 1.5 nm (within 1  $\times$  1  $\mu$ m area) for bare cells to 3.5 nm for cells encapsulated in (silk)<sub>8</sub> shells (Figure 5, Figure S3). Fine domain texture for silk shells is typical for silk materials with

a significant amount of  $\beta$ -sheets, which are aggregated in nanoscale domains.<sup>[28]</sup> A highly grainy surface morphology suggests a potentially porous morphology of the silk shells. The pore sizes might possibly reach 20 nm as was measured for similar silk microcapsules after methanol treatment.<sup>[28]</sup> The high permeability of the silk shells is essential for transporting the nutrients and for the proper response to physiological changes.

Next, the ability of cells to function and reproduce after LbL encapsulation over time was monitored with turbidity density measurements, which display traditional S-shape behavior (**Figure 6**). The half-period of bare cell growth was consistently observed to be around 16 hours. Growth kinetics of coated cells that have been treated with a mild concentration of K<sup>+</sup> phosphate buffer showed no changes in the ability of cells to replicate, with a small delay (by two hours or about 10% change) in reaching the maximum rate of log phase (Figure 6a). Incubation of encapsulated cells treated with the phosphate buffer of higher concentration (0.1 M) led to an additional delay of another two hours in reaching the stationary phase, suggesting that silk structure transformation with increased concentration of ions directly affects the functionality encapsulated cells, consistently leading to reduced metabolic function. The ability of cells to bud (produce daughter cells) demonstrates the strength of cells or the ability to withstand mechanical constraints after the process of encapsulation. It also demonstrates the non-cytotoxic properties of silk nanoshells without compromising the cell viability and metabolic activities. Accumulation of yeast enhanced green fluorescent protein (yEGFP) production in response to the inducer molecule (2% galactose), assessed by measuring fluorescence from green fluorescent protein (GFP) expression of

yEGFP over time, further confirmed normal cell functioning with insignificant (only a few hours) lag (Figure 6b). A paired t-test revealed statistically insignificant difference (level of confidence  $\alpha = 0.05$ ) in GFP expression between control and encapsulated cells (regardless of salt strength treatment) within the tested time range.

A minimal delay in reaching the stationary phase and unaltered yEGFP expression suggests that silk shells can efficiently preserve inherited functionality of cells in contrast with cells encapsulated in synthetic polymer shells.<sup>[8]</sup> Indeed, in comparison to polymer nanoshells, these “silked” cells demonstrated significantly higher response rates and shorter lag times.<sup>[8]</sup> A relatively fast response to the inducer

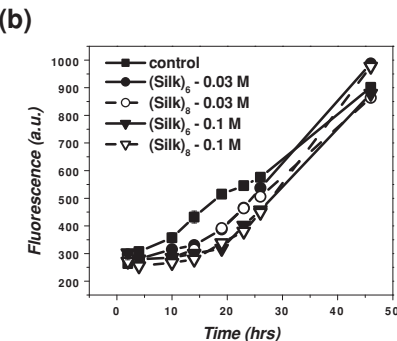
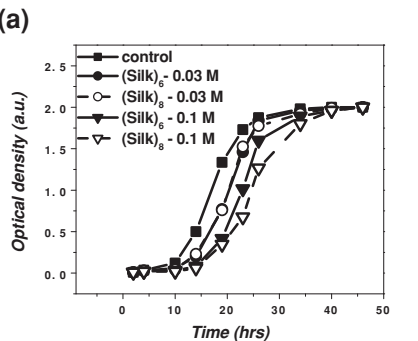


**Figure 6.** Growth kinetics (a) and expression of yEGFP (b) of yeast cells encapsulated in 6 or 8 layers of silk ((Silk)<sub>6</sub> and (Silk)<sub>8</sub>, respectively) and treated with 0.03 M or 0.1 M of K<sup>+</sup> phosphate buffer after each layer in comparison to uncoated (control) cells.

molecules and as a result, synthesis of the yEGFP, demonstrates the integrity and unaltered functionality of encapsulated yeast cells, and it can be considered as proof of preserved metabolic activity. Factors such as high biocompatibility of the salting-out process of silk protein along with high porosity of the shells might be responsible for higher viability and unaltered cellular function, which are rarely achieved with synthetic polymer shells.<sup>[8]</sup>

The confocal images taken after encapsulation and throughout the log phase at different times displayed a gradual change in “silked” cell morphology (**Figures 7, S4**). Immediately after encapsulation, the red fluorescent silk shell is clearly observed as a thin red shell surrounding the peripheral part of the cell (**Figures 7, S4**). During cell maturation after incubation in media supplemented with yEGFP inducer molecules (12 h), it appears that the labeled protein diffuses through the periphery of the cell.

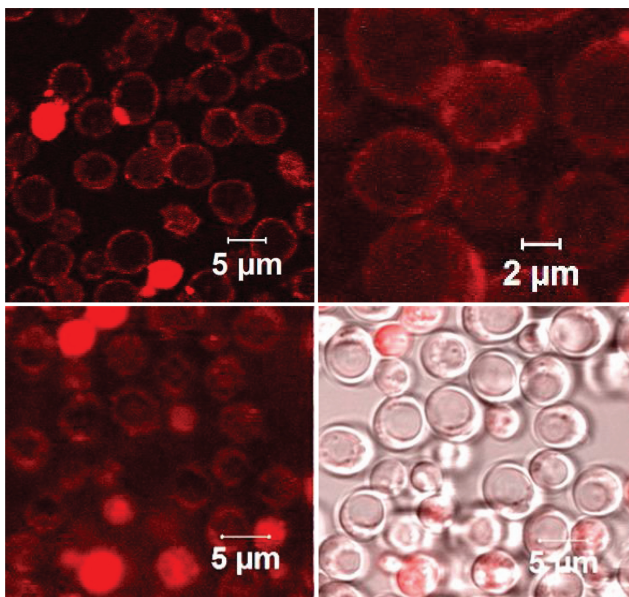


**Figure 7.** Confocal fluorescent images of encapsulated in (Silk)<sub>8</sub> yeast cells before incubation (top) and after 12 h (bottom) of incubation in media supplemented with 2% galactose to induce yEGFP expression. Bottom right images represents overlap of fluorescent and optical images for cell identification.

At the half-period of maximum growth (18 h), “silked” cells showed no presence of the clearly defined shell, while red fluorescence was mostly observable within the interior of the cell (**Figures 8, S5**). By the time when cells reached the stationary phase in their growth behavior (25 h), we observed significant reduction in red fluorescence, most likely associated with degradation of silk protein onto the smaller fragments. Particularly, a higher concentration of residuals from labeled silk was found to be accumulated in the cell vacuole, a type of lysosome responsible for recycling of misfolded proteins and storing the waste (**Figure 8, S5**).<sup>[51]</sup>

We suggest that during active metabolic activity, which was not affected by the presence of the silk protein shell, partial degradation of silk occurs during exocytosis of waste products (mainly CO<sub>2</sub>, and ethyl alcohol) (**Figure 1**). Indeed, silk protein undergoes secondary structure transitions when acidity is increasing (CO<sub>2</sub> acts as a volatile acid) or during partial dehydration, promoting β-sheet content.<sup>[41,52]</sup> These peripheral reactions might promote endocytosis of degraded silk fibroin fragments, as was only observed for short protein fragments (usually 20–35 residues length).<sup>[53]</sup> It is worth to note that the release of free dye molecules can be completely excluded because dye is covalently attached to the amine-bearing side chains of silk fibroin which is also exhaustively dialyzed against Nanopure water to remove any unbound free dye molecules (see Experimental). Moreover, no penetration of free unbound fluorescent dye inside of the healthy cells was observed at these stages for many hours after cell encapsulation but only after cell reproduction. In order to quantify the degradation profile of the silk layer with other methods, the uptake mechanism should be identified by monitoring degradation and internalization of proteins, which can be a subject of future research.

### 3. Conclusion

In conclusion, we demonstrated highly efficient cell encapsulation with cytocompatible, stable, and biodegradable nanoshells constructed from locked in silk fibroin. Very high, never observed before viability rates (up to 97%) along with preserved high metabolic activity of “silked” cells were achieved due to a greater cytocompatibility of very thin and highly porous silk nanoshells. Successful stabilization of silk protein shells during the salting-out procedure was achieved by the proper salt treatment with incubation in buffer. Moreover, in a striking contrast with traditional synthetic shells these protein nanoshells, after serving as nanoshells for cell encapsulation, undergo fast biodegradation and digestion, leaving behind mature cells with full functionality and no trace of the initial shells.

We further suggest that functionalization of silk nanoshells with DNA, antigens, or enzymes via inherent bioactive motifs can potentially generate biologically active cells

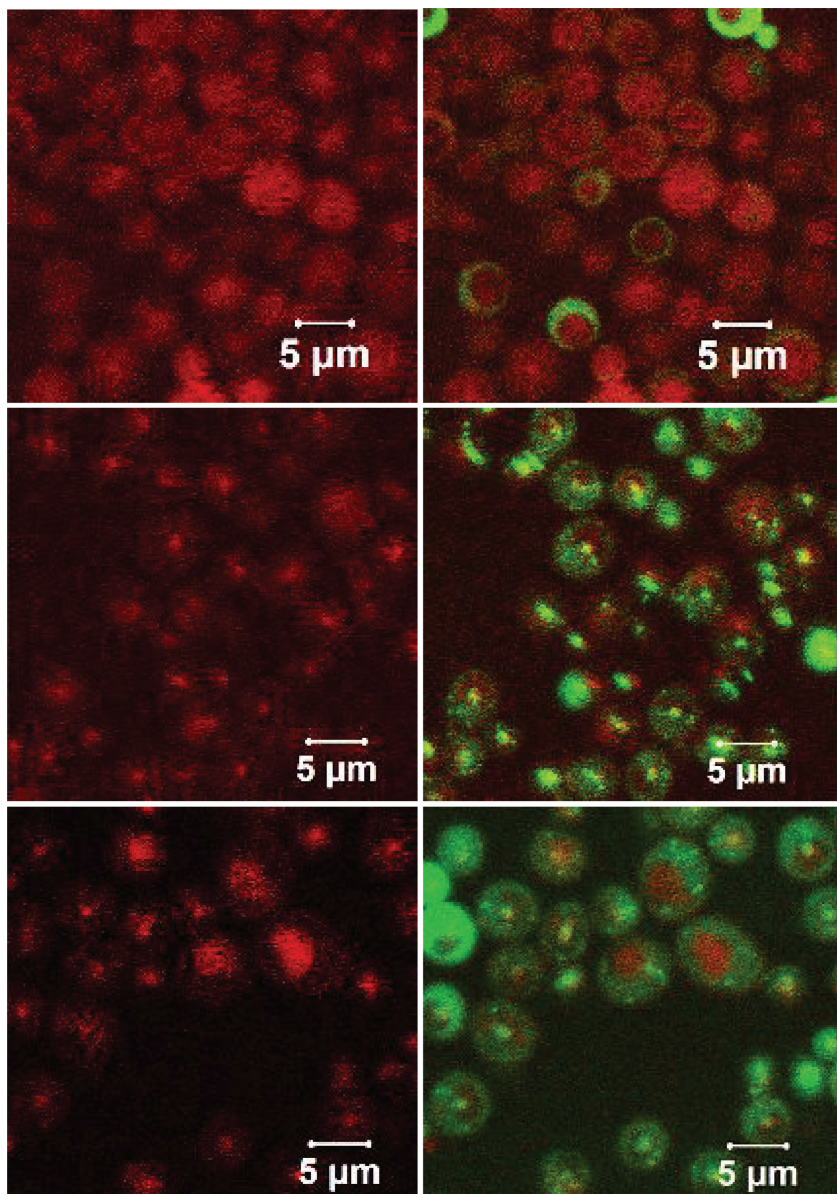


**Figure 8.** Confocal fluorescent images of encapsulated in (silk)<sub>8</sub> yeast cells at 18, 20, and 25 h (from top to bottom) after incubation in media supplemented with 2% galactose to induce yEGFP expression. Left column represents gradual internalization of fluorescently labeled silk (red) inside of the cells. Right column (starting from 18 h) represents colocalization of yEGFP expression (green) within the interior of the cell with fluorescently labeled silk (red).

and controlled temporarily protected cells for implantation. Hence, the biodegradable silk nanoshells introduced here can be considered as an efficient way to provide short-term protection for the cells during implantation without affecting their metabolic activity, and they display higher biodegradability compared to traditional synthetic shells that have been fabricated to date. These ultrathin protective LbL shells from biocompatible natural materials can be considered for a wide range of applications. Proper selection of chemical composition and assembling conditions dramatically increases the viability of encapsulated cells and increase their stability, robustness, and resistance to the external disturbances and aggressive environment. The minute thickness of these

shells, controlled permeability and eventual biodegradability which facilitates cell release from shells at well-defined conditions important for highly sensitive biosensing and integration into biological environments.

#### 4. Experimental Section

**Materials:** Mono- and dibasic sodium and potassium phosphates, sodium chloride and other chemicals used in the study were purchased from Sigma-Aldrich. Nanopure (Barnstead Nanopure system) water with a resistivity of 18.2 MΩ cm was used in all experiments.

**Silk purification:** Silk fibroin aqueous stock solutions were prepared as previously described.<sup>[54,55]</sup> Briefly, cocoons were boiled for 20 min in an aqueous solution of 0.02 M sodium bicarbonate and then rinsed thoroughly with Nanopure water to extract the glue-like sericin proteins. The extracted silk fibroin was dissolved in 9.3 M LiBr solution at 60 °C for 4 h, yielding a 20% (w/v) solution. The solution was dialyzed against Nanopure water using Slide-a-Lyzer dialysis cassettes (molecular weight cutoff (MWCO) 3500, Pierce) at room temperature overnight to remove the LiBr. The dialysate was centrifuged three times, each at 20 °C for 20 min to remove impurities and the aggregates that occurred during dialysis. The 4% (w/v) dialysate solution was filtered using 0.4 μm glass-fiber syringe filters. The final concentration of reconstituted silk fibroin solution was diluted with Nanopure water to yield 0.1% aqueous silk solution.

**Synthesis of Silk-co-Alexa532:** Aqueous solution of silk (0.2% w/v) was combined with aqueous solution of Alexa Fluor 532 (*N*-hydroxysuccinimidyl ester) fluorescent dye in a 15:1 ratio. The mixture was kept in a cold water bath overnight with slow stirring to produce silk-co-Alexa532 fluorescently labeled silk. The solution of silk-co-Alexa532 was exhaustively dialyzed against Nanopure water for 4 days using Slide-a-Lyser dialysis cassettes to remove any unbound fluorescent dye and was used directly on the top of the pre-formed silk shells.<sup>[8]</sup>

**Yeast Cells:** The *Saccharomyces cerevisiae* YPH501 diploid yeast strain expressing a plasmid encoding yeast-enhanced green fluorescent protein (yEGFP) as a biomarker was used for this study.<sup>[8]</sup> Cells were cultured in a synthetic minimal medium (SMM) supplemented with 2% glucose solution. Yeast cells were grown at 30 °C in a shaker incubator (New Brunswick Scientific) set to 220 rpm in order to bring them to an early exponential phase when the optical density reached 0.4–0.5 a.u. based on a 0–2 a.u. scale (absorbance was measured at 600 nm on a GE cell calculator).

**Encapsulation of *Saccharomyces cerevisiae* Yeast Cells with Reconstituted Silk:** LbL assembly was employed for encapsulation of yeast cells in accordance with the procedure applied earlier (Figure 1).<sup>[28]</sup> Before deposition of silk, cells were extensively washed in Na<sup>+</sup> phosphate buffer (0.01 M, pH 6) and centrifuged down at 1000 rpm to collect loose pellet. Silk layers (designated as (silk)<sub>n</sub>, where *n* denotes the number of layers) were allowed to absorb on cell surfaces from aqueous solution (1 mg mL<sup>-1</sup>, pH 5) for 10 min by gentle rotation at 35 rpm. After deposition of silk, cells were collected by centrifugation at 1000 rpm and washed with Nanopure water to remove any unbound silk protein, followed by incubation in Na<sup>+</sup> or K<sup>+</sup> phosphate buffer solutions (0.03 M pH 5.5, or 0.1 M pH 5.5) for 10 min. To induce transition of silk fibroin from random coil to  $\beta$ -sheet cells were incubated by vigorous shaking on Vertex (1000 rpm). The final washing was done in Nanopure water, after which the next deposition step of silk was performed. The formation of stable silk-on-silk shells around cells was induced by an all-aqueous salting-out process after deposition of every silk layer (Figure 1).<sup>[28,37]</sup>

**Cell Viability:** Cell viability was assessed immediately after the encapsulation process with Live-Dead and resazurin assay kits according to manufacturer's protocols (BioVision).<sup>[56]</sup> For the Live-Dead test, representative images were collected with a Zeiss 510 UV LSM using a band-pass filter ( $\lambda_{Ex/Em} = 488/515$  and  $\lambda_{Ex/Em} = 543/560$  nm for detection of FITC and Rhodamine, respectively). Confocal micrographs were analyzed with *ImageJ* software to quantify the number of live (green) and dead (red) cells. For the resazurin-based assay, fluorescence was measured at  $\lambda_{Em} = 585$  nm ( $\lambda_{Ex} = 560$  nm) on a spectrofluorophotometer (Shimadzu RF 5301 PC) after incubation for 4 h.

**Cell Growth and Expression of yEGFP:** Encapsulated cells were incubated in 2% raffinose and 2% galactose in SMM yeast media at 30 °C to induce the yEGFP production. Optical density (or cell turbidity) at  $\lambda = 600$  nm (OD600) and fluorescence at  $\lambda_{Em} = 515$  nm ( $\lambda_{Ex} = 480$  nm) were measured at indicated time points. A paired two sample t-test for means was performed to check the difference in yEGFP expression between control and encapsulated cells within the sampled time range.

**Characterization:** The surface morphology of the silk-modified yeast cells in the dry state was characterized with atomic force microscopy (AFM) according to the established procedure.<sup>[57]</sup> The topographical and phase images were collected on Icon (Bruker) in light-tapping mode using scan-assisted V-shape cantilevers with a spring constant of 46 N/m. Scanning electron microscopy (SEM) of air-dried cells was performed on a Hitachi S-3400-II electron microscope at 10 kV. Before imaging, cells were fixed with a 4% gluteraldehyde buffered solution (0.1 M Na<sup>+</sup> phosphate, pH 7.4), air-dried on silicon wafers, and sputtered with gold.

Dynamic light scattering (DLS) experiments and  $\zeta$ -potential measurements of silk fibroin at different pH values were performed using a Nanoseries Zetasizer Nano-ZS (Malvern). Silk solution was mixed with potassium phosphate of different molarities in volumetric ratios of 1:6 using a pipette. For DLS measurements, back-light scattering using refractive indices of 1.33 and 1.6 for buffer and protein solutions respectively were selected. Each  $\zeta$ -potential value was obtained at ambient conditions by averaging three independent measurements of 35 sub-runs each.

Ellipsometry measurements were employed to estimate the thickness of LbL silk films in the dry state using a M-2000U

spectroscopic ellipsometer (Woolam). Silk films were deposited from aqueous solutions (1 mg mL<sup>-1</sup>, pH 5.0) using the dip-assisted method for 10 minutes and then were briefly incubated in solutions of either 0.03 M phosphate buffer (pH 5.3), 0.1M K<sup>+</sup> phosphate buffers (pH 5.3), or in Nanopure water (negative control), or 100% methanol (positive control).

Confocal laser scanning microscopy (CLSM) images of yeast cells encapsulated with different bilayer architecture were obtained on a LSM 510 UV Vis inverted laser scanning microscope equipped with a 63  $\times$  1.4 oil immersion objective lens (Zeiss). To visualize the shell around the cells, silk-co-Alexa532 was deposited as a top layer (1 mg mL<sup>-1</sup>, 0.01 M phosphate buffer, pH 6.5). For co-localization of shell and fluorescence from yEGFP, encapsulated cells were incubated in 2% galactose at 30 °C to induce yEGFP expression. Cells were visualized using excitation/emission wavelengths of 488/515 nm for detection of yEGFP and 543/560 nm for detection of silk-co-Alexa532.

## Supporting Information

Supporting Information is available from the Wiley Online Library or from the author. It includes viability rates of yeast cells encapsulated in silk nanoshells treated with K<sup>+</sup> or Na<sup>+</sup> phosphate buffers of different molarities (Figure S1); comparative thickness of silk films in dry state treated with Nanopure water, phosphate buffers of different strength and methanol (Figure S2); SEM and AFM images of uncoated yeast cells (Figure S3); confocal images (in color) of yeast cells encapsulated in silk protein shells before and after incubation in media for 12 h (Figure S4); time elapsed confocal images (in color) of yeast cells during gradual internalization of silk protein coating (Figure S5).

## Acknowledgements

The study is supported by grants FA9550-11-1-0233 and FA9550-09-1-0162 (BIONIC Center) from Air Force Office Of Scientific Research. We acknowledge Chunhong Ye for some AFM images and Kesong Hu for silk purification. We thank Prof. V. T. Milam (GaTech) for providing access to Zeta-sizer.

- [1] G. Decher, *Layer-by-Layer Assembly (Putting Molecules to Work)*, in *Multilayer Thin Films: Sequential Assembly of Nanocomposite Materials*, 2<sup>nd</sup> ed. (Eds: G. Decher, J. B. Schlenoff), Wiley-VCH Verlag GmbH & Co. KGaA, Weinheim, Germany 2012.
- [2] G. H. Altman, F. Diaz, C. Jakuba, T. Calabro, R. L. Horan, J. Chen, H. Lu, J. Richmond, D. L. Kaplan, *Biomaterials* **2003**, 24, 401.
- [3] J. Velema, D. L. Kaplan, *Adv. Biochem. Eng. Biotechnol.* **2006**, 102, 187.
- [4] M. Matsusaki, K. Kadokawa, Y. Nakahara, M. Akashi, *Angew. Chem.* **2007**, 119, 4773.
- [5] a) R. F. Fakhrullin, Y. M. Lvov, *ACS Nano* **2012**, 6, 4557; b) R. F. Fakhrullin, A. I. Zamaleeva, R. T. Minullina, S. A. Konnova, V. N. Paunov, *Chem. Soc. Rev.* **2012**, 41, 4189; c) A. Diaspro, D. Silvano, S. Krol, O. Cavalleri, A. Gliozzi, *Langmuir* **2002**, 18,

- 5047; d) D. Volodkin, A. Skirtach, H. Möhwald, *Adv. Polym. Sci.* **2011**, 240, 135; e) B. G. De Geest, G. B. Sukhorukov, H. Möhwald, *Expert Opin. Drug Delivery* **2009**, 6, 613; f) C. Jiang, V. V. Tsukruk, *Adv. Mater.* **2006**, 18, 829.
- [6] H. F. Hildebrand, N. Blanchemain, G. Mayer, F. Chai, M. Lefebvre, F. Boschin, *Surf. Coat. Technol.* **2006**, 200, 6318.
- [7] Y. Lvov, K. Ariga, I. Ichinose, T. Kunitake, *J. Am. Chem. Soc.* **1995**, 117, 6117.
- [8] a) I. Drachuk, O. Shchepelina, M. Lisunova, S. Harbaugh, N. Kelley-Loughnane, M. Stone, V. V. Tsukruk, *ACS Nano* **2012**, 6, 4266; b) V. Kozlovska, S. Harbaugh, I. Drachuk, O. Shchepelina, N. Kelley-Loughnane, M. Stone, V. V. Tsukruk, *Soft Matter* **2011**, 7, 2364; c) J. T. Wilson, W. Cui, V. Kozlovska, E. Kharlampieva, D. Pan, Z. Qu, V. R. Krishnamurthy, J. Mets, V. Kumar, J. Wen, Y. Song, V. V. Tsukruk, E. L. Chaikof, *J. Am. Chem. Soc.* **2011**, 133, 7054; d) J. L. Carter, I. Drachuk, S. Harbaugh, N. Kelley-Loughnane, M. Stone, V. V. Tsukruk, *Macromol. Biosci.* **2011**, 11, 1244.
- [9] a) C. Jiang, V. V. Tsukruk, *Soft Matter* **2005**, 1, 334; b) C. Jiang, B. M. Rybak, S. Markutsya, P. E. Kladitis, V. V. Tsukruk, *Appl. Phys. Lett.* **2005**, 86, 121912.
- [10] A. A. Antipov, G. B. Sukhorukov, *Adv. Colloid Interface Sci.* **2004**, 111, 49.
- [11] a) S. A. Morin, R. F. Shepherd, S. W. Kwok, A. A. Stokes, A. Nemiroski, G. M. Whitesides, *Science* **2012**, 337, 828; b) R. V. Martinez, C. R. Fish, X. Chen, G. M. Whitesides, *Adv. Funct. Mater.* **2012**, 22, 1376; c) R. F. Shepherd, F. Ilievski, W. Choi, S. A. Morin, A. A. Stokes, A. D. Mazzeo, X. Chen, M. Wang, G. M. Whitesides, *Proc. Natl. Acad. Sci. USA* **2011**, 108, 20400.
- [12] Y. Cui, S. N. Kim, R. R. Naik, M. C. McAlpine, *Acc. Chem. Res.* **2012**, 45, 696.
- [13] K. D. Anderson, R. B. Weber, M. E. McConney, H. Jiang, T. J. Bunning, V. V. Tsukruk, *Polymer* **2012**, 53, 4686.
- [14] R. A. Potyrailo, N. Nagraj, C. Surman, H. Boudries, H. Lai, J. M. Slocik, N. Kelley-Loughnane, R. R. Naik, *Trends Anal. Chem.* **2012**, 40, 133.
- [15] J. C. Harper, T. L. Edwards, T. Savage, S. Harbaugh, N. Kelley-Loughnane, M. O. Stone, C. J. Brinker, S. M. Brozik, *Small* **2012**, 8, 2743.
- [16] D. M. Eby, S. Harbaugh, R. N. Tatum, K. E. Farrington, N. Kelley-Loughnane, G. R. Johnson, *Langmuir* **2012**, 28, 10521.
- [17] a) S. H. Yang, S. M. Kang, K.-B. Lee, T. D. Chung, H. Lee, I. S. Choi, *J. Am. Chem. Soc.* **2011**, 133, 2795; b) J. Gensel, T. Borke, N. P. Perez, A. Fery, D. V. Andreeva, E. Betthausen, A. H. E. Muller, H. Mohwald, E. V. Skorb, *Adv. Mater.* **2012**, 24, 985.
- [18] N. Nugaeva, K. Y. Gfeller, N. Backmann, H. P. Lang, M. Düggelin, M. Hegner, *Biosens. Bioelectron.* **2005**, 21, 849.
- [19] L. E. de-Bashan, J. P. Hernandez, T. Morey, Y. Bashan, *Water Res.* **2004**, 38, 466;
- [20] a) P. H. G. Chao, S. Yodmuang, X. Wang, L. Sun, D. L. Kaplan, G. Vunjak-Novakovic, *J. Biomed. Mater. Res., B* **2010**, 95, 84; b) A. R. Murphy, P. S. John, D. L. Kaplan, *Biomaterials* **2008**, 29, 2829.
- [21] a) C. Vepari, D. L. Kaplan, *Prog. Polym. Sci.* **2007**, 32, 991; b) A. Leal-Egaña, T. Scheibel, *Biotechnol. Appl. Biochem.* **2010**, 55, 155; c) L. Eisoldt, A. Smith, T. Scheibel, *Mater. Today* **2011**, 14, 80; d) F. Vollrath, *Nature* **2010**, 466, 319; e) H. Jin, D. L. Kaplan, *Nature* **2003**, 424, 1057; f) M. Xu, R. V. Lewis, *Proc. Natl. Acad. Sci. USA* **1990**, 87, 7120; g) M. J. Buehler, Y. C. Yung, *Nat. Mater.* **2009**, 8, 175.
- [22] X. Wang, J. A. Kluge, G. G. Leisk, D. L. Kaplan, *Biomaterials* **2008**, 29, 1054.
- [23] M. Haider, J. Cappello, N. Ghandehari, K. L. Leong, *Pharm. Res.* **2008**, 25, 692.
- [24] a) C. Jiang, X. Wang, R. Gunawidjaja, Y.-H. Lin, M. K. Gupta, D. L. Kaplan, R. R. Naik, V. V. Tsukruk, *Adv. Funct. Mater.* **2007**, 17, 2229; b) E. Kharlampieva, D. Zimnitsky, M. Gupta, K. N. Bergman, D. L. Kaplan, R. R. Naik, V. V. Tsukruk, *Chem. Mater.* **2009**, 21, 2696; c) E. Kharlampieva, V. Kozlovska, B. Wallet, V. V. Shevchenko, R. R. Naik, R. Vaia, D. L. Kaplan, V. V. Tsukruk, *ACS Nano* **2010**, 4, 7053; d) E. Kharlampieva, V. Kozlovska, R. Gunawidjaja, V. V. Shevchenko, R. Vaia, R. R. Naik, D. L. Kaplan, V. V. Tsukruk, *Adv. Funct. Mater.* **2010**, 20, 840.
- [25] E. Ruiz-Hitzky, K. Ariga, Y. Lvov, *Bio-inorganic Hybrid Nanomaterials: Strategies, Syntheses, Characterization and Applications*, Wiley-VCH, Weinheim, Germany **2008**.
- [26] V. Kozlovska, S. Yakovlev, M. Libera, S. A. Sukhishvili, *Macromolecules* **2005**, 38, 4828.
- [27] V. Kozlovska, E. Kharlampieva, I. Drachuk, D. Cheng, V. V. Tsukruk, *Soft Matter* **2010**, 6, 3596.
- [28] O. Shchepelina, I. Drachuk, M. K. Gupta, J. Lin, V. V. Tsukruk, *Adv. Mater.* **2011**, 23, 4655.
- [29] J. T. Wilson, W. Cui, E. L. Chaikof, *Nano Lett.* **2008**, 8, 1940.
- [30] a) K. Ariga, H. Ito, J. P. Hill, H. Tsukube, *Chem. Soc. Rev.* **2012**, 41, 5800; b) H. Ai, M. Fang, S. A. Jones, Y. M. Lvov, *Biomacromolecules* **2002**, 3, 560.
- [31] F. Caruso, D. Trau, H. Mohwald, R. Renneberg, *Langmuir* **2000**, 16, 1485.
- [32] M. L. Macdonald, R. E. Samuel, N. J. Shah, R. F. Padera, Y. M. Beben, P. T. Hammond, *Biomaterials* **2011**, 32, 1446.
- [33] J. T. Wilson, V. R. Krishnamurthy, W. Cui, Z. Qu, E. L. Chaikof, *J. Am. Chem. Soc.* **2009**, 131, 18228.
- [34] A. Pantos, D. Tsiourvas, C. M. Paleos, G. Nounesis, *Langmuir* **2005**, 21, 6696.
- [35] A. N. Zelikin, *ACS Nano* **2010**, 4, 2494.
- [36] D. Mertz, H. Wu, J. S. Wong, J. Cui, P. Tan, R. Alles, F. Caruso, *J. Mater. Chem.* **2012**, 22, 21434.
- [37] L. Eisoldt, J. G. Hardy, M. Heim, T. R. Scheibel, *J. Struct. Biol.* **2010**, 170, 413.
- [38] C. Wong Po Foo, E. Bini, J. Hensman, D. P. Knight, R. V. Lewis, D. L. Kaplan, *Appl. Phys. A: Mater. Sci. Process.* **2006**, 82, 223.
- [39] T. Yucel, P. Cebe, D. L. Kaplan, *Biophys. J.* **2009**, 97, 2044.
- [40] C. Ye, O. Shchepelina, R. Calabrese, I. Drachuk, D. L. Kaplan, V. V. Tsukruk, *Biomacromolecules* **2011**, 12, 4319.
- [41] a) S. L. Young, M. Gupta, C. Hanske, A. Fery, T. Scheibel, V. V. Tsukruk, *Biomacromolecules* **2012**, 13, 3189; b) B. Wallet, E. Kharlampieva, K. Campbell-Proszowska, V. Kozlovska, S. Malak, J. F. Ankner, D. L. Kaplan, V. V. Tsukruk, *Langmuir* **2012**, 28, 11481; c) M. K. Gupta, S. Singamaneni, M. McConney, L. F. Drummy, R. R. Naik, V. V. Tsukruk, *Adv. Mater.* **2010**, 22, 115.
- [42] T. Yucel, C. M. Micklitsch, J. P. Schneider, D. J. Pochan, *Macromolecules* **2008**, 41, 5763.
- [43] U. J. Kim, J. Park, C. Li, H.-J. Jin, R. Valluzzi, D. L. Kaplan, *Biomacromolecules* **2004**, 5, 786.
- [44] G. Karp, *Cell and Molecular Biology. Concepts and Experiments*, 4th Ed., John Wiley & Sons, Inc., USA **2005**, p.156.
- [45] L. Vrbka, J. Vondrasek, B. Jagoda-Cwiklik, R. Vacha, P. Jungwirth, *Proc. Natl. Acad. Sci. USA* **2006**, 103, 15440.
- [46] A. L. Serdakowski, J. S. Dordick, *Trends Biotechnol.* **2008**, 26, 48.
- [47] A. S. Lammel, X. Hu, S. H. Park, D. L. Kaplan, T. R. Scheibel, *Biomaterials* **2010**, 31, 4583.
- [48] F. Hagn, C. Thamm, T. Scheibel, H. Kessler, *Angew. Chem. Int. Ed.* **2011**, 50, 310.
- [49] A. Matsumoto, J. Chen, A. L. Collette, U.-J. Kim, G. H. Altman, P. Cebe, D. L. Kaplan, *J. Phys. Chem. B* **2006**, 110, 21630.
- [50] P. Chen, H. S. Kim, C.-Y. Park, H.-S. Kim, I.-J. Chin, H.-J. Jin, *Macromol. Res.* **2008**, 16, 539.
- [51] G. M. Walker, *Yeast Physiology and Biotechnology*, Wiley-VCH, Weinheim, Germany **1998**.
- [52] M. L. Floren, S. Spilimbergo, A. Motta, C. Migliaresi, *Biomacromolecules* **2012**, 13, 2060.
- [53] K. A. Brogden, *Nat. Rev. Microbiol.* **2005**, 3, 238.

- [54] D. M. Phillips, L. F. Drummy, D. G. Conrady, D. M. Fox, R. R. Naik, M. O. Stone, P. C. Trulove, H. C. De Long, R. A. Mantz, *J. Am. Chem. Soc.* **2004**, *126*, 14350.
- [55] D. M. Phillips, L. F. Drummy, R. R. Naik, H. C. De Long, D. M. Fox, P. C. Trulove, R. A. Mantz, *J. Mater. Chem.* **2005**, *15*, 4206.
- [56] Cellviabilityassaykits:<http://www.biovision.com/manuals/K501.pdf>, <http://www.biovision.com/manuals/K303.pdf>, accessed: October, 2012.
- [57] a) V. V. Tsukruk, S. Singamaneni, *Scanning Probe Microscopy of Soft Matter: Fundamentals and Practices*, Wiley-VCH, Weinheim, Germany 2012; b) M. E. McConney, S. Singamaneni, V. V. Tsukruk, *Polym. Rev.* **2010**, *50*, 235.

Received: November 30, 2012

Revised: January 7, 2013

Published online: April 18, 2013